Biophysical Journal Volume 102 February 2012 887–896

An Atomistic View on Human Hemoglobin Carbon Monoxide Migration Processes

M. Fátima Lucas[†] and Víctor Guallar[†‡*]
[†]Joint BSC-IRB Research Program in Computational Biology, Barcelona Supercomputing Center, Barcelona, Spain; and [‡]Institució Catalana de Recerca i Estudis Avançats (ICREA), Barcelona, Spain

ABSTRACT A significant amount of work has been devoted to obtaining a detailed atomistic knowledge of the human hemoglobin mechanism. Despite this impressive research, to date, the ligand diffusion processes remain unclear and controversial. Using recently developed computational techniques, PELE, we are capable of addressing the ligand migration processes. First, the methodology was tested on myoglobin's CO migration, and the results were compared with the wealth of theoretical and experimental studies. Then, we explored both hemoglobin tense and relaxed states and identified the differences between the α-and β-subunits. Our results indicate that the proximal site, equivalent to the Xe1 cavity in myoglobin, is never visited. Furthermore, strategically positioned residues alter the diffusion processes within hemoglobin's subunits and suggest that multiple pathways exist, especially diversified in the α-globins. A significant dependency of the ligand dynamics on the tertiary structure is also observed.

INTRODUCTION

Globins are heme-containing proteins involved in the transport and storage of molecular oxygen (O_2). For many years, myoglobin (Mb) has been the preferentially studied globin both experimentally and theoretically (1–5). Capable of reversible oxygenation, it has served as a prototype for structure-function relationship studies of more complex systems. Hemoglobin (Hb), in contrast, constitutes a challenge for the study of protein structural dynamics, given its complexity and cooperativity effects between subunits. Adult human hemoglobin is a tetrameric ($\alpha_1\beta_2\ \alpha_2\beta_1$) protein containing two different subunits called α-globin and β-globin, each of which holds a heme group. The binding pocket, similar in both globins, protects the iron atom from the solvent, and for this reason, it is essential for ligands to migrate from solution through the protein to reach the active site. Examination of their crystal structures, however, does not show any obvious channels for diffusion, and so it has become clear that protein flexibility is required (6–8).

The processes by which ligands gain access to the active site has been a subject of research for many years, and it is now well known that internal cavities play an important role (3,9). These are normally packing defects that reduce the overall thermodynamic stability of a protein (10,11), and it has been postulated that their presence must have a functional purpose (12,13). In Mb, the most important of these intermediate docking sites are commonly known as the distal site and the xenon (Xe) cavities, Xe1 (located at the proximal site)–Xe4 (9). Once the ligand (O_2, CO, etc.) is dissociated from the iron, the primary docking site is found in the distal pocket, where the ligand remains oriented parallel to the heme plane, above the porphyrin pyrrole C ring (14). Photodissociated CO has also been observed at secondary docking positions that coincide with two of the xenon-binding sites (namely Xe1 and Xe4) (15–17) and several passageways and bottlenecks between paths have been uncovered. The idea that the progress of the ligand in and out of the protein involves the rotation of the side chain of the distal histidine 64 (E7) was proposed over 40 years ago by Perutz et al (18). This histidine-gated hypothesis was later supported on experimental work (19–22), and it is now recognized that the commonly known distal pathway is comprised of Leu-29, Phe-33, Phe-43, Phe-46, His-64, and Val-68. Most studies indicate that this is the most favorable and shortest pathway for ligands to reach or escape the heme (20). In addition, there is evidence for other paths on the distal side of the protein as well as passing by the experimentally observed xenon sites (23,24).

Many years of intense research was necessary to unravel the putative network of pathways known nowadays in Mb (3,25–29). A quick search through the literature, on the other hand, shows a scarce amount of information on diffusion pathways in Hb. The complexity of the structure makes it difficult to extract experimental information and limits the use of theoretical tools. Work by Birukou et al., in which the distal histidine was replaced by several amino acids, shows differences between Hb's subunits (30,31). Geminate and bimolecular rate studies on several mutants—Leu(b10), Val(E11) and Leu(G8), all present in the distal pocket in both α-and β-units—seems to favor the existence of one main exit from the protein (32). At the theoretical level, a study by Mouawad et al. (33) has been reported on human Hb using steered molecular dynamics (MD), where the formation of transient internal cavities and passageways has been reported. Further work on a smaller dimeric Hb of *Scapharca inaequivalvis* also proposed the existence of

Submitted September 14, 2011, and accepted for publication January 11, 2012.

*Correspondence: victor.guallar@bsc.es

Editor: Bert de Groot.

0006-3495/12/02/0887/10 $2.00

doi: 10.1016/j.bpj.2012.01.011

several cavities (34). Sovino et al. report that α-and β-chains exposed to high-pressure Xe display heterogeneous behavior (35). A work just made available, where unbiased MD simulations were performed on the isolated α-chain of Hb, shows internal hydrophobic pockets and evaluates ligand rebinding kinetics (36).

Here, we have used PELE (Protein Energy Landscape Exploration), a recently developed technique, to present a complete atomistic exploration of the CO migration in human Hb as well as Mb, which was used as a test system. PELE combines a Monte Carlo stochastic approach with protein structure prediction algorithms, and it is capable of accurately reproducing long-timescale processes in only a few hours of CPU (37–39). We have applied PELE on the high-affinity R state and the low-affinity T state, and have assessed the differences in diffusion processes. Hemoglobin's α-and β-units were investigated individually, and the results show that the two chains are different not only structurally but also functionally. We have identified passages by the distal side equivalent to the ones found in Mb and show a set of other alternatives for the ligand's escape.

METHODS

In this work, PELE is used to map carbon monoxide entry/escape routes in Mb and Hb. The long-timescale dynamics associated with these processes are easily accessible to PELE because this program combines a steered stochastic approach with protein structure prediction methods. The algorithm involves the consecutive iteration of three main moves: a ligand and protein (backbone) perturbation, a side-chain sampling, and a minimization (40,41) The procedure begins by generating a local perturbation to the ligand and/or the protein. Ligand perturbation involves a translation and rotation of the center of mass of the ligand. Protein perturbations are based on the displacement of α-carbon according to an anisotropic network model (ANM), a simple model for normal-mode analysis (42). The α-carbons are displaced based on a randomly picked low eigenvector (or a combination of them) obtained in the ANM approach. The system is then minimized with a harmonic constraint on each displaced α-carbon. The algorithm is also capable of pinpointing the most excited side chains, i.e., the ones experiencing the largest changes in energy as a consequence of the ANM move. These are then included in the subsequent side-chain prediction step. For the side-chain sampling, the algorithm proceeds by optimally arranging all side chains local to the ligand (within a determined distance), as well as the hot side chains identified in the ANM step (40,41). In practice, the distance to and number of hot side chains are adjusted so that the total number of side chains does not exceed 25; larger groups of side chains will result in poor predictions. The last stage involves the minimization of a region including, at least, all residues local to the atoms involved in steps 1 and 2. These three steps compose a move that is accepted (defining a new minimum) or rejected based on a Metropolis criterion for a given temperature. The collection of accepted steps forms a stochastic trajectory. The combination of ligand and protein backbone perturbations results in an effective exploration of the protein energy landscape (PES) that is capable of reproducing large conformational changes associated with ligand migration and has already been shown to produce reliable results (37,38). In particular, the methodology has been very effective in reproducing diatomic ligand migration in bacterial Hbs (38). PELE uses an OPLS (Optimized Potentials for Liquid Simulations) all-atom force field (43) with an implicit surface-generalized Born (SGB) continuum solvent model (44).

Hb and Mb setup

Initial coordinates for the T-state (CO-unligated) and R-state (CO-ligated) structures were taken from Protein Data Bank (PDB) entries 1A3N (45) and 1BBB (46), respectively. The CO-ligated Mb structure was obtained from two structures identified with PDB entries 1A6G (5) and 2MB5 (47). An unligated state was also investigated in which the initial structure was taken from the protein database with the entry 1A6N (5). Preparation of the protein structures was assisted by the protein preparation wizard in the Schrödinger package (48). All missing hydrogen atoms were added, and residues such as arginines and lysines were set to have cationic side chains, whereas glutamate and aspartate were established to be anionic, in agreement with the neutral physiological pH. Histidines were visually inspected and assigned to be delta, epsilon, or doubly protonated in function of their nearby environment. In particular, Hb His-146 in the β-chains is known to play a special role, as the higher pH present in peripheral tissues favors its protonation with release of O_2 and the shift to the preferred T state. For this reason, the tense state was modeled with a fully protonated histidine 146, whereas in the R state only the delta nitrogen was protonated (49,50).

In the bound R state, the CO-Fe bond interaction of the chain under study was removed and the system was minimized within PELE. The parameters for the heme's bound and unbound states were derived by quantum mechanical/molecular mechanical (QM/MM) geometry optimizations (see below). In the case of the unligated T state, the CO was also initially placed in the vicinity of the heme. Two different approaches were adopted: 1), a ligand migration to the active site from the CD loop area (using PELE); and 2), a direct insertion of the ligand in the heme cavity followed by side-chain sampling and minimization. No significant differences in the free ligand exploration were observed with either method.

For each state, 40 independent trajectories were produced. Each simulation used eight processors, which moved together in exploring the PES such that if one processor found a different area (4 Å away from the average position), all the other processors would follow it and all processors would continue the exploration together. The simulations stopped when the ligand reached solution.

CO-phenylalanine correction

Based on the existing evidence of the importance of phenylalanine residues in ligand migration (29,37), in addition to picosecond time-resolved x-ray crystallographic studies (51), we investigated the accuracy of the force field's description of the CO-Phe stacking interactions. First, we performed some test calculations (available in Fig. S1 and Fig. S2 in the Supporting Material) to establish the acceptable level of theory to be used and verified that the MP2 (52) with the basis set aug-cc-pvtζ was adequate for the calculations (53). We then prepared 15 models that consisted of a benzene ring, where CO molecules were placed at five different positions and at three different distances relative to the ring. We found that the strongest interaction for the ligand, ~2 kcal/mol, is in the middle of the ring at 3.5 Å, in agreement with calculations performed with the ligand free to optimize. For each model, we compared MP2 and PELE's OPLS all-atom force-field interaction energies and realized that the minimum is 50% underestimated, by ~1 kcal/mol, when using the classical force field. We have corrected this interaction by adding an attractive Gaussian term between a phenylalanine ring and a CO molecule at the center of the ring:

$$Energy = A \times e^{B(r-C)^2},$$

where A, B, and C adopted the values of -1.0, -0.2, and 3.0, respectively.

In Fig. 1, we can observe two short simulations with (*right*) and without (*left*) the correction term. It is clear that the new potential stabilizes the ligand near the phenylalanine close to the center of the benzene ring, as is expected from the MP2 calculations.

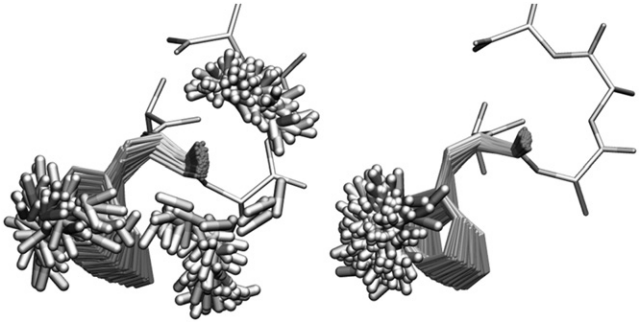

FIGURE 1 CO digression near a system composed of three residues, the central residue being a phenylalanine. The older version of PELE software was used for the structure on the left, where the corrected versioni was used for the righthand structure.

QM/MM calculations

Parameters for all heme structures were derived from QM/MM calculations. For this, a 10-Å water box was added and equilibrated. Finally, a single snapshot is selected and all waters except for a layer of ~8 Å around the protein are removed. For these particular calculations, the quantum region consisted of the heme and proximal histidines in the case of the unbound system. For the hexa-coordinated system, a carbon monoxide group was also included. These systems were allowed to relax in the protein matrix, where all residues within 15 Å were free, and a complete optimization was performed with the QSite (54) QM/MM software. The density functional method B3LYP (55–59) with the lacvp* (60) (for Fe atoms) and 6-31G* (61) (for all other atoms) basis sets is used for the quantum layer, and the OPLS force field (43) is used for the classical part. A singlet-state Fe^{2+} is established for the bound state and a quintet state is used for the unbound state. The electrostatic-potential partial charges were included in the templates for the heme containing all necessary bonding and nonbonding parameters (all data are available in the Supporting Material).

RESULTS

In the first part of this section, the CO ligand migration in Mb will be revisited. An exhaustive study is presented that also serves to validate the methodology, given the large amount of experimental and theoretical data available for this system. The second part comprises the study of Hb ligand migration processes.

Myoglobin

We have initiated the work by exploring Mb's CO escape paths. As mentioned in the Methods section, we have added a correction to the force field used in PELE to adequately describe the phenylalanine-CO stacking interactions. Sixty independent simulations were performed (using the 1A6G structure) with and without the corrections, allowing the ligand to move freely out of the protein. The nature of the paths, and the frequency at which the ligand leaves by each exit, are very similar with either version of the force field. However, a main difference arises in the amount of time that the ligand spends in the proximity of the phenylalanine site. We find that the phenylalanine site, formed by Phe-33, Phe-43, and Phe-46, is visited in 61% of the trajectories when the corrected potential is used compared to 34% with the uncorrected potential. We observe that the proximal site, the Xe1 cavity, is visited more frequently (and for longer times) with the corrected force field. This is expected, given that for the ligand to explore the proximal side of the protein it must pass over Phe-138. Long residency times in Xe1 are in agreement with crystallographic studies (15,17,62). Furthermore, the slow geminate recombination phase observed in Mb has been attributed to rebinding after visiting this inner cavity (20). Thus, we believe that the introduced correction describes in a more accurate way the real dynamics of these systems. For this reason, and due to the better agreement with MP2 calculations, all the Hb simulations were performed using the corrected version of the force field (Fig. 2).

Fig. 2 shows the different ligand migration paths found with PELE, along with the experimentally known xenon sites. The ligand initially populates the primary docking site (within 4 Å of the iron (Fe) atom—constrained by Leu-29, Leu-32, His-64, Ile-107, and Val-68), where it remains above the pyrrole C, parallel to the heme plane. From this point, the ligand has been seen to escape in 63% of the simulations between the heme D propionates and Phe-43, also known as the distal path (Fig. 2, *green*). These results are in good agreement with kinetic analyses that suggest that ~70–80% of the ligands leave by this pathway (20,63). In some of these trajectories, the side chain

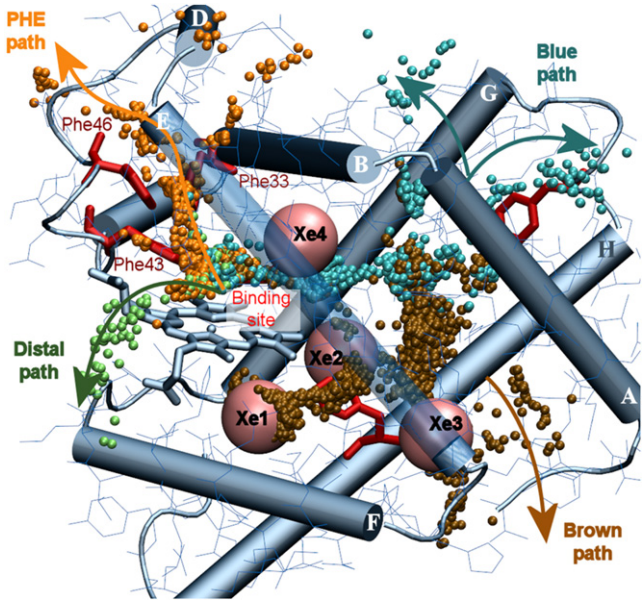

FIGURE 2 View of the carbon monoxide exit passages in Mb. The protein is shown in cartoon representation with most of the helices labeled. The ligand, in bead representation, indicates the center of mass of the molecule. Different colors specify the different exit paths, and the pink spheres identify the xenon sites.

of the distal His-64 rotates to allow the passage of the ligand, also consistent with the histidine gate hypothesis (18). We also found what we will call here the phenylalanine pathway (PHE path), similarly observed in previous calculations (4,29,37), having as portal residues Leu-29, Phe-33, and Phe-43 (Fig. 2, *orange*). Going in the opposite direction, and passing by the Xe4 site, the ligand escapes at the AB helix corner (passing through both sides of the G helix) by the path identified in blue. For the exit on the left side (to the B helix side in Fig. 2), it is necessary for Arg-118 to undergo considerable side-chain movement, whereas on the right side (toward helix A), the His-119 allows the passage of the ligand to the solvent. In the case of the paths shown in Fig. 2, in brown, 17% of the trajectories find their exit near the EF corner, passing the Xe3 site or in the proximity of the A helix. The four docking sites are identified in the figure: Xe1 on the proximal side of the heme, Xe2 next to Xe1 and Phe-128, Xe3 close to the EF corner, and Xe4 on the distal side (Fig. 2, *pink spheres*; the cavities are represented as identical spheres for simplicity purposes only and do not represent the actual size or shape of the cavities).

In addition to 1A6G, we have also investigated ligand migration processes for two other initial Mb structures. The two systems correspond to another ligated structure, 2MB5 (used also in a previous MD study by Ruscio et al. (64)), and an unligated (apo) structure, 1A6N. Calculations show that the passages in all these systems are identical, with only the addition of a new path found in 2MB5 (with a frequency of $<10\%$), where the ligand exits by the proximal side of the heme after visiting the Xe1 site. This passage was not seen in the calculations with the other ligated structure, 1A6G, but interestingly, it was reported in the Ruscio et al. MD study (64) using 2MB5 as initial coordinates. The frequency with which each passage is taken, however, changes considerably when comparing the ligated or unligated structures. For the other initial ligated state, 2MB5, the main exit path is found to be by the distal path (~53%); thus, together with the phenylalanine path, this accounts for 70% of the exits by the distal side, in close agreement with the 1A6G simulation. The unligated state presents a reduced digression through the distal path with only 12.5% choosing this gate. The main exits, previously identified as the brown and blue paths, with 42.5% and 22.5%, respectively, occur through the protein matrix. These differences between ligated and unligated states will be further debated in the Discussion section.

An impressive amount of experimental and theoretical data are available in literature on Mb's ligand diffusion processes. Single-mutation studies have shown that the substitution of His-64, Phe-43, and Phe-46 for a smaller residue leads to an increase in the rate constant for O_2 entry, which supports the importance of these residues in the histidine gate hypothesis (20). However, the replacement of these amino acids by tryptophan does not annihilate ligand binding, which puts forward the idea of other possible pathways. Furthermore, it has been shown that the escape rates of the ligand are not significantly affected by a considerable number of single mutations. Scott and Gibson demonstrated that filling the Xe1 and Xe4 sites with xenon gas eliminated the slow phases observed for geminate rebinding but produced little change in the total amount of geminate recombination, which could explain the small effect on single mutations of residues away from the heme (65). This evidence seems to open the possibility of several pathways with similar affinity for the ligand's escape. This is further supported by the work by Huang and Boxer (24), where clusters of residues were mutated simultaneously.

In addition to experimental studies, much computational work has also been dedicated to the research of ligand migration processes in Mb. Both theoretical and experimental information seem to point to the coexistence of several paths, but the ligand appears to have a preferential escape route by the distal path (4,20,22,24,28,37,66–71). A recent article (71), where the CO diffusion process was investigated by reconstructing a three-dimensional potential-of-mean-force landscape on fully atomistic MD simulation, shows all minima in agreement with the distal pocket and xenon sites. An extensive MD study performed by Ruscio et al. (64) also identifies the distal path as the preferential exit and entrance passage occurring in ~50% of the simulations. As indicated above, when using the same initial coordinates we obtain a quantitative agreement, with 53% of exits by the distal path. Thus, the pathway analysis exploration with PELE is equivalent to that produced with long MD, but at a fraction of the computational cost. For Mb, each trajectory took ~10 h. With four processors, this added up to 40 CPU h/trajectory, thus requiring 2400 CPU h for 60 trajectories run, which is ~4 days in a 24 CPU cluster. Furthermore, since the methodology involves mostly local perturbations (ligand translation, side-chain prediction of residues around the ligand, etc.), it does scale nicely with size, making it an ideal tool to target complex systems like human Hb.

Hemoglobin

In this section, we will present the ligand diffusion processes for human Hb using PELE. The high-affinity, ligated (R) and the low-affinity unligated (T) states, as well as the α-and β-units, were studied. We produced 40 independent trajectories for each system. During the simulation, backbone perturbation is only added to the chain where the ligand is dissociated. Thus, only tertiary changes are allowed in the chain under study, with the overall quaternary structure being fairly constant throughout the simulation. In short simulations, i.e., when the ligand escapes quickly to the solvent, we do not observe considerable changes in the protein's tertiary structure, but in extended simulations, where the ligand remains trapped in the protein matrix longer, the scission of the Fe-CO bond and consequent retraction of the

proximal histidine induces changes in the nearby EF chains. The E chain is seen to approach the heme site, whereas the F chain moves away from it. This tertiary movement is observed in the crystals along the R-to-T transition and has been clearly characterized in Mb (72).

Ligated R state

α-Globin

Just as we observed for Mb, the ligand, initially in the active site, explores the distal cavity and is limited by the presence of residues His-58, Val-62, Leu-29, and Leu-101. We find that from 40 trajectories, 35% of the time, the CO molecule escapes the protein by the PHE path site. The ligand moves to the phenylalanine cavity close to Phe-33 and Phe-43 and exits the protein between Lys-40 and Leu-48. There are two possibilities for bypassing Phe-33, either between the three phenylalanines—33, 43, and 46—or behind Phe-33. In Fig. 3, we can see the main paths found, as well as the exit frequencies for both the R and T states of Hb's α-and β-chains.

We have also found that in 7% of the simulations, the ligand molecule escapes from between the heme D propionate and Phe-43, surpassing the proximal histidine over the C and D pyrrole rings. This passage is equivalent to the distal path in Mb and is shown in green in Fig. 3. There are a number of different migration pathways that explore

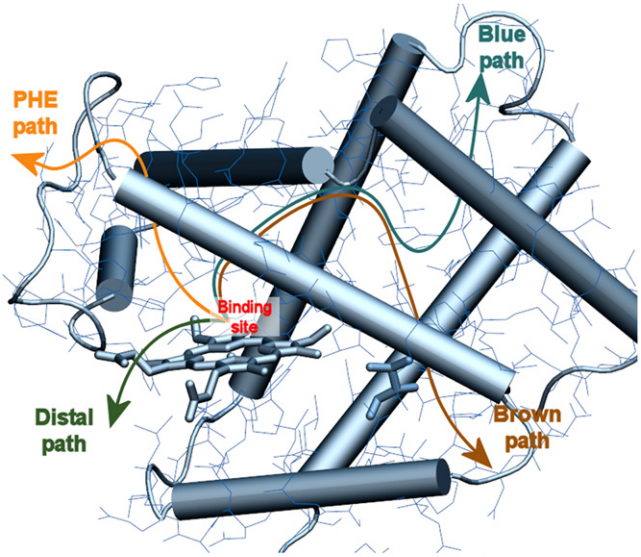

	Rα	Rβ	Tα	Tβ
Distal path	7.5	95.0	22.5	57.5
PHE path	35.0	-	12.5	<5
Brown path	17.5	-	22.5	<5
Blue path	22.5	5.0	35.0	30.0
others	17.5	-	7.5	7.5

FIGURE 3 Schematic representation of the carbon monoxide exit passages in human Hb. The table contains information concerning the percentage of ligands that exit by each path shown in the figure.

the interior of the protein, the combination of which represent almost 60% of the trajectories. In all situations, the ligand starts by exploring a cavity bordered by residues Gly-25, Val-62, Leu-101, and Leu-105. From here, the ligand can escape by the brown path between the G and H helices, where it finds the solvent or moves into the internal $\alpha_2\beta_2$ cavity of Hb. Fig. S5 shows the exploration of the interior of the protein and the exit. The other path shown in blue explores a second large cavity comprised of the residues Trp-14, Ala-21, Val-70, Leu-105, and Leu-109. Trp-14 exhibits large movements of the side chain to allow the ligand to be accommodated in this cavity. In the blue path, the ligand exits near the AB corner.

For the Hb Rα state we find that the ligand never explores the proximal site. Our results show that for Mb, in all instances where the proximal side of the heme is visited, Phe-138 must move to allow the ligand's passage. This residue appears to have a gate function to that flank of the heme, which has been seen before in MD simulations (70). Hb, in contrast, does not have this phenylalanine, and instead, Val-132 is found in an equivalent position for the α-unit.

β-Globin

The diffusion processes in Rβ Hb indicate essentially only one main pathway, the distal path (95%), with only 5% of the trajectories moving toward the inner side of the protein.

The ligand begins by occupying the distal pocket, where it remains (as always) parallel to the heme. In this globin, the exit by the distal path follows two possible trends: the ligand can move close to Phe-41 and Phe-42 over the pyrrole ring D or, on the other side of the heme, over pyrrole A, exiting in the vicinity of the A propionate. We also observe that in some simulations, the ligand resides close to Phe-42 and Phe-45, occupying the phenylalanine site but never exiting from the CD loop. In addition to the distal path, on very few occasions, we also see the ligand exiting close to the AB corner, shown in blue in Figs. 2 and 3. To probe for the existence of cavities in this unit, we performed 10 additional simulations, taking the initial position of CO from this last trajectory close to Leu-106 and Leu-110, since the quick exit by the distal path reduced the probability of finding the ligand inside the protein. In this way, we were able to identify a cavity flanked by Leu-68, Leu-106, Leu-110, Phe-71, Ala-138, and Leu-141, as well as the escape tunnel (blue trajectory) gated by Trp-15 close to the AB corner. This cavity is similar to the one found in Rα and has no equivalent in Mb.

Unligated T state

α-Globin

In 12% of the simulations, the ligand exited by the PHE path through the CD loop next to Leu-48 after exploring

the phenylalanine site. The distal path is taken in a total of 22% of the trajectories, with the ligand exiting by either side of the distal histidine. When the ligand explores the interior of the protein, a first small cavity is encountered identical to the one seen previously in the R state. This comprises the residues Gly-25, Val-62, Leu-101, and Leu-105, and digression of the ligand from here can occur in two directions: toward a second cavity near the GH corner or toward the Val-132 that blocks the passage to the proximal site. The second cavity also resembles the ones seen in the relaxed state and is surrounded by the residues Trp-14, Ala-21, Val-70, Leu-105, and Leu-109. This cavity is highly explored by the most popular exit passage, represented in blue (Fig. 3). In this case, we observe that 35% of the trajectories choose this path and exit between the AB and the GH corners. We have also observed ligand escape by a passage similar to the previously identified brown path, but in this case, the ligand moves toward the solvent and not into the protein as seen in most cases in the R state.

β-Globin

The systematic exploration of the exit paths for the tense state's β-subunit proved to be considerably different from those for the α-subunit, just as we have already seen for the R conformation. Out of 40 simulations, we observed that in 58% of the trajectories, the ligand escapes by the distal path. In 30% of the cases, the ligand explored the blue path and on very few occasions, the carbon monoxide exited by the brown and phenylalanine paths.

A small hydrophobic pocket similar to that seen for the other subunits is found. The cavity is surrounded by the residues Leu-68, Leu-106, Leu-110, Phe-71, Ala-138, and Leu-141, the latter responsible for blocking the passage of the ligand toward the proximal site.

DISCUSSION

In the previous section, we presented a full atomistic description of the escape passages found for Mb and Hb using PELE. We have used Mb as a model system and studied three initial structures: two ligated states and one unligated. The results show that Mb exhibits a diversified network of passages that are independent of the initial structure. Essentially, four exits are found for carbon monoxide: the distal path commonly accepted as the principal escape from the protein's active site; the phenylalanine path; and two exits that explore the inner part of the protein, here referred to as brown and blue paths. Differences occur in the frequency at which each path is taken. For the ligated states, we find prevalence for exit by the distal path (63% and 53% of the trajectories), in good agreement with experimental observations (20,63). On the other hand, when the unligated state is studied, the distal path is taken less frequently (a tendency also observed in Hb), with dominance of the brown exit, close to the Xe3 cavity.

These results clearly indicate that ligand migration is significantly coupled to the tertiary structure. Together with Professor Spiro, we previously showed that the main tertiary change during ligand binding involves a concerted rotation in the E and F helix (72). In particular, in the unligated structure, the E helix collapses toward the active site. We observe here that this collapse partially blocks the migration of the ligand to the distal site (pushing the ligand to the interior of the protein). The importance of the tertiary structure in ligand dynamics was also reported in exquisite sol-gel encapsulating experiments by the Friedman group (73). Although our sampling protocol is capable of observing tertiary R-to-T transitions (as mentioned above), a description of the reverse direction would necessarily involve modeling the ligand binding into the iron center. Independent of the initial state, our results strongly support the existence of multiple paths, in agreement with computational and most experimental data (25). We were able to confirm the histidine gate hypothesis and identify all xenon sites.

The investigation performed on Hb's subunits displayed diffusion processes noticeably unlike those from Mb. One of the main differences between the two globins is the exploration of the proximal site. This site, identified in Mb as the Xe1 cavity, is never visited in Hb. Inspection of Mb's escape paths shows that whenever the proximal site is visited, Phe-138 must rotate its side chain, thus functioning as a gate. Hemoglobin, instead, has a valine (132) and a leucine (141) for the α-and β-units, respectively. The phenylalanine side chain is able to perform large rotations, whereas the valine and leucine are essentially rigid. These differences in structure explain the absence of migration processes to the proximal side of the protein, which is known to be more compact (33,74). As mentioned above, in Mb, the slow phase of geminate rebinding is attributed to the exploration of this cavity. Interestingly, in Hb the geminate rebinding is considerably faster ($>100\ \mu s^{-1}$, as shown recently in Birukou et al. (32)) than in Mb, in agreement with the lack of proximal-site exploration.

Substantial variances between the α-and β-subunits are also observed. The main statistics from these studies are summarized in Fig. 4.

It is clear that significant differences arise depending on the subunit under study. The main exit pathway for both β-chains is by the distal site (including here all paths leaving from the distal site, namely, the distal and PHE paths), especially relevant in the Rβ state, where the digression of the ligand toward the protein matrix is negligible (5%). This favorable exit by the distal path for the β-chains seems to result from a combination of factors. The CO molecule can leave either between the A and D propionate or the neighboring Phe-42 and Ser-44 close to the CD loop; thus, the existence of alternative routes should facilitate departure from the distal path. In addition, the restricted access inside the protein seems to be the consequence of the proximity of

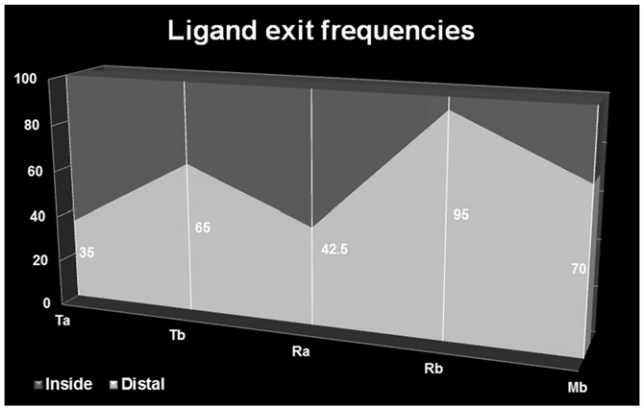

FIGURE 4 Overall statistics for ligand migration from the active site to the exterior of the protein. Mb and the R and T states for Hb are shown, as are the α-and β-subunits.

the residues Leu-110, Leu-68, Leu-106, and Val-67. In particular, the position of Leu-68 is identical to that of the smaller Ala-63 present in the α-chains. Alternatively, the α-chains seem to have an intricate network of passages exploring the protein inner cavities. Furthermore, a limited number of exits by the distal path are found in these globins. The existence of a hydrogen bond between the carboxylate group from heme D propionate and His-45, in a position equivalent to those of Ser-44 and Asp-44 in the β-unit and Mb, respectively, limits the movement of the ligand in this direction. An alternative passage, particularly in the case of the Rα unit, is through the PHE path, mostly absent in the β-chains given the replacement of Phe-33 by Leu-32 in Mb and the α-chains. The dissimilar behavior of these two chains was already shown experimentally, where geminate rebinding studies point to nonequivalence of the two subunits (75,76). The different exploration of inner cavities in the two chains is also supported by recent high-pressure Xe studies. Birukou et al. showed, for the α-chain, an increase in the fraction of geminate recombination from 0.28 to 0.43 when adding 4 atm of Xe gas (32). The β-chain did not show any major difference (decreasing from 0.33 to 0.32). In a similar way, the escape rate for the α-chain decreased from 24 to 17 μs^{-1} (again, no significant change is observed in the β-chain). Altogether, the data clearly indicate a larger inner cavity exploration in the α-chain. An exhaustive study on mutations (glycine, alanine, leucine, glutamine, phenylalanine, and tryptophan) of the distal histidine also reveals differences between the two subunits (30). In the β-subunits, the rate constant for bimolecular O_2 binding decreases with increasing size of the amino acid, supporting the idea that the distal histidine acts as the main gate. However, Birukou et al. (30) find that the bimolecular rate constant for the α-globins is more complex.

Supporting the hypothesis of multiple pathways, a very recent study (36) that combines MD simulations and laser kinetic spectroscopy reveals the presence of several transient cavities in the α-subunit of an isolated Hb. The theoretical study included 140 independent trajectories that display four main exits. In addition to the traditional distal path, an exit occurring by what they refer to as the phantom Ph1 site resembles the PHE path found here and also reported previously for Mb. In addition, two other routes lead into the protein matrix, occupying several docking sites, consistent with the kinetic model proposed. Our results for the α-subunit T state also show four possible exit passages, in excellent agreement with the unbiased MD study. For the Rα state, all paths are identical to those found in the T state, but in addition, we found digression of the ligand to the interunit cavity.

Comparing the results for the different Hb states, we find again a systematic increase in the exits by the distal side when going from the T to the R state. In the case of the α-chains, the increase is 35–42.5%, whereas for the β-chain, an increase from 65% to 95% is observed. As discussed above for Mb, this increase correlates with the tertiary displacement (along the T-to-R transition) of the E helix with respect to the heme group (72). In the R structure, the helix is located farther away from the heme prosthetic group, facilitating ligand migration in the distal site.

Mb was seen to present four main cavities, consistent with the experimentally observed xenon cavities. Hb, however, shows a more compact proximal site. In the case of the β-chain, we see that when the ligand explores the interior of the protein it often becomes trapped in a cavity in close proximity to Phe-71. Shibayama et al. (74) reported that photodissociated CO molecules in the β-subunits of the T state Hb are located in two sites, the distal pocket and a hydrophobic cavity in the back of the distal pocket, ~8.5 Å away from the iron. This cavity is not seen in Mb, and inspection of the crystal structure shows the pocket taken by Leu-72, with the rigid side chain occupying the space of the phenylalanine's labile benzene ring. The α-subunits also have a leucine in this same position, but it is placed farther away from the heme CBB atom, thus allowing enough free space for the ligand to occupy. For the α-chains, in addition to this first cavity, the ligand is also found in a second very large pocket placed between the AB and the GH corners. The existence of inner cavities close to the distal pocket has been reported previously (33,35,74,77). Investigation of xenon sites in horse Hb (78) showed a very different pattern compared to Mb. Two xenon sites were found: one in chain α-and one in the β-unit, lying in slightly different positions. The xenon atom in the α-chain is nearer to the GH corner and that in the β-chain is closer to the AB corner. More recently, xenon sites identified in human Hb show very few cavities in the β-chains, whereas, according to the authors, the α-chains are populated by a "constellation of sites" that can map potential paths between the active site and solution (35).

In summary, to the best of our knowledge, this is the first complete mapping of human Hb's diatomic ligand pathways.

The tense and relaxed states were investigated, and the two subunits, α and β, were compared. An atomist view is provided that pinpoints the principal residues involved in the migration pathways. We find considerable differences between the α-and β-chains in either conformational state. The β-chain in both the T and R states appear to have a preference for exit by the distal path, with few incursions toward the protein's matrix. Alternatively, the α-chains display a more complex network of possible exits. In addition to exit by the distal site, digressions toward the inside of the protein are observed. We find heterogeneity of the two globins repeatedly reported in both experimental and theoretical studies, and we confirm that unlike those of Mb, subunits of Hb are not open for CO migration to the proximal site. A significant dependency of the ligand dynamics with the tertiary structure is also observed.

The calculations performed with PELE display results in good agreement with the available experimental and theoretical data. The low computational cost of this method allows for its application in complex systems such as Hb.

SUPPORTING MATERIAL

Model systems used in the CO-phenylalanine correction, comparison of the interaction energies using different basis set within MP2 theory, template files for the ligated and unligated heme groups, comparison between the ligand diffusion processes of three myoglobin initial pdb structures, comparison between the results from PELE on myoglobin and a study by Huang and Boxer, ligand exploration for the Rα subunit, and five figures and two references are available at http://www.biophysj.org/biophysj/supplemental/S0006-3495(12)00084-7.

Computational resources were provided by the Barcelona Supercomputing Center.

This work was supported by funds from the Barcelona Supercomputer Center and the ERC-2009-Adg 25027-PELE European project. M.F.L. was supported by The Fundação para a Ciência e Tecnologia, grant SFRH/BPD/47901/2008.

REFERENCES

1. Kendrew, J. C., R. E. Dickerson, …, V. C. Shore. 1960. Structure of myoglobin: a three-dimensional Fourier synthesis at 2 Å resolution. *Nature*. 185:422–427.
2. Austin, R. H., K. W. Beeson, …, I. C. Gunsalus. 1975. Dynamics of ligand binding to myoglobin. *Biochemistry.* 14:5355–5373.
3. Brunori, M., D. Bourgeois, and B. Vallone. 2004. The structural dynamics of myoglobin. *J. Struct. Biol.* 147:223–234.
4. Elber, R., and M. Karplus. 1990. Enhanced sampling in molecular dynamics: use of the time-dependent Hartree approximation for a simulation of carbon monoxide diffusion through myoblobin. *J. Am. Chem. Soc.* 112:9161–9175.
5. Vojtechovský, J., K. Chu, …, I. Schlichting. 1999. Crystal structures of myoglobin-ligand complexes at near-atomic resolution. *Biophys. J.* 77:2153–2174.
6. Kuriyan, J., S. Wilz, …, G. A. Petsko. 1986. X-ray structure and refinement of carbon-monoxy (Fe II)-myoglobin at 1.5 Å resolution. *J. Mol. Biol.* 192:133–154.
7. Phillips, S. E. V. 1980. Structure and refinement of oxymyoglobin at 1.6 Å resolution. *J. Mol. Biol.* 142:531–554.
8. Takano, T. 1977. Structure of myoglobin refined at 2·0 Å resolution. II. Structure of deoxymyoglobin from sperm whale. *J. Mol. Biol.* 110:569–584.
9. Tilton, R. F., I. D. Kuntz, and G. A. Petsko. 1984. Cavities in proteins: structure of a metmyoglobin-xenon complex solved to 1.9 Å. *Biochemistry.* 23:2849–2857.
10. Anderson, D. E., J. H. Hurley, …, B. W. Matthews. 1993. Hydrophobic core repacking and aromatic-aromatic interaction in the thermostable mutant of T4 lysozyme Ser 117—>Phe. *Protein Sci.* 2:1285–1290.
11. Hasegawa, J., H. Shimahara, …, Y. Igarashi. 1999. Stabilization of *Pseudomonas aeruginosa* cytochrome *c*(551) by systematic amino acid substitutions based on the structure of thermophilic *Hydrogenobacter thermophilus* cytochrome *c*(552). *J. Biol. Chem.* 274:37533–37537.
12. Brunori, M., and Q. H. Gibson. 2001. Cavities and packing defects in the structural dynamics of myoglobin. *EMBO Rep.* 2:674–679.
13. Tomita, A., U. Kreutzer, …, T. Jue. 2010. 'It's hollow': the function of pores within myoglobin. *J. Exp. Biol.* 213:2748–2754.
14. Lim, M., T. A. Jackson, and P. A. Anfinrud. 1997. Ultrafast rotation and trapping of carbon monoxide dissociated from myoglobin. *Nat. Struct. Biol.* 4:209–214.
15. Brunori, M., B. Vallone, …, I. Schlichting. 2000. The role of cavities in protein dynamics: crystal structure of a photolytic intermediate of a mutant myoglobin. *Proc. Natl. Acad. Sci. USA*. 97:2058–2063.
16. Ostermann, A., R. Waschipky, …, G. U. Nienhaus. 2000. Ligand binding and conformational motions in myoglobin. *Nature.* 404: 205–208.
17. Chu, K., J. Vojtchovský, …, I. Schlichting. 2000. Structure of a ligand-binding intermediate in wild-type carbonmonoxy myoglobin. *Nature.* 403:921–923.
18. Perutz, M. F., and F. S. Mathews. 1966. An x-ray study of azide methaemoglobin. *J. Mol. Biol.* 21:199–202.
19. Bolognesi, M., E. Cannillo, …, M. Brunori. 1982. Reactivity of ferric Aplysia and sperm whale myoglobins towards imidazole. X-ray and binding study. *J. Mol. Biol.* 158:305–315.
20. Scott, E. E., Q. H. Gibson, and J. S. Olson. 2001. Mapping the pathways for O2 entry into and exit from myoglobin. *J. Biol. Chem.* 276:5177–5188.
21. Springer, B. A., K. D. Egeberg, …, J. S. Olson. 1989. Discrimination between oxygen and carbon monoxide and inhibition of autooxidation by myoglobin. Site-directed mutagenesis of the distal histidine. *J. Biol. Chem.* 264:3057–3060.
22. Rohlfs, R. J., A. J. Mathews, …, S. G. Sligar. 1990. The effects of amino acid substitution at position E7 (residue 64) on the kinetics of ligand binding to sperm whale myoglobin. *J. Biol. Chem.* 265:3168–3176.
23. Tilton, Jr., R. F., U. C. Singh, …, P. A. Kollman. 1988. Protein-ligand dynamics. A 96 picosecond simulation of a myoglobin-xenon complex. *J. Mol. Biol.* 199:195–211.
24. Huang, X., and S. G. Boxer. 1994. Discovery of new ligand binding pathways in myoglobin by random mutagenesis. *Nat. Struct. Biol.* 1:226–229.
25. Elber, R. 2010. Ligand diffusion in globins: simulations versus experiment. *Curr. Opin. Struct. Biol.* 20:162–167.
26. Danielsson, J., P. Banushkina, …, M. Meuwly. 2006. Computer simulations of structures, energetics and dynamics of myoglobin···ligand complexes. *Int. Rev. Phys. Chem.* 25:407–425.
27. Bossa, C., A. Amadei, …, A. Di Nola. 2005. Molecular dynamics simulation of sperm whale myoglobin: effects of mutations and trapped CO on the structure and dynamics of cavities. *Biophys. J.* 89:465–474.
28. Olson, J. S., and G. N. Phillips, Jr. 1996. Kinetic pathways and barriers for ligand binding to myoglobin. *J. Biol. Chem.* 271:17593–17596.

29. Cohen, J., A. Arkhipov, …, K. Schulten. 2006. Imaging the migration pathways for O2, CO, NO, and Xe inside myoglobin. *Biophys. J.* 91:1844–1857.
30. Birukou, I., R. L. Schweers, and J. S. Olson. 2010. Distal histidine stabilizes bound O2 and acts as a gate for ligand entry in both subunits of adult human hemoglobin. *J. Biol. Chem.* 285:8840–8854.
31. Birukou, I., J. Soman, and J. S. Olson. 2011. Blocking the gate to ligand entry in human hemoglobin. *J. Biol. Chem.* 286:10515–10529.
32. Birukou, I., D. H. Maillett, A. Birukova, and J. S. Olson. 2011. Modulating distal cavities in the $\alpha$and β subunits of human HbA reveals the primary ligand migration pathway. *Biochemistry.* 50:7361–7364.
33. Mouawad, L., J.-D. Maréchal, and D. Perahia. 2005. Internal cavities and ligand passageways in human hemoglobin characterized by molecular dynamics simulations. *Biochim. Biophys. Acta.* 1724:385–393.
34. Nienhaus, K., J. E. Knapp, …, G. U. Nienhaus. 2007. Ligand migration and binding in the dimeric hemoglobin of *Scapharca inaequivalvis*. *Biochemistry.* 46:14018–14031.
35. Savino, C., A. E. Miele, …, B. Vallone. 2009. Pattern of cavities in globins: the case of human hemoglobin. *Biopolymers.* 91:1097–1107.
36. Lepeshkevich, S. V., S. A. Biziuk, …, B. M. Dzhagarov. 2011. The kinetics of molecular oxygen migration in the isolated α chains of human hemoglobin as revealed by molecular dynamics simulations and laser kinetic spectroscopy. *Biochim. Biophys. Acta.* 1814:1279–1288.
37. Borrelli, K. W., A. Vitalis, …, V. Guallar. 2005. PELE: Protein energy landscape exploration. A novel Monte Carlo based technique. *J. Chem. Theory Comput.* 1:1304.
38. Guallar, V., C. Lu, …, S. R. Yeh. 2009. Ligand migration in the truncated hemoglobin-II from *Mycobacterium tuberculosis*: the role of G8 tryptophan. *J. Biol. Chem.* 284:3106–3116.
39. Hernández-Ortega, A., K. Borrelli, …, V. Guallar. 2011. Substrate diffusion and oxidation in GMC oxidoreductases: an experimental and computational study on fungal aryl-alcohol oxidase. *Biochem. J.* 436:341–350.
40. Jacobson, M. P., R. A. Friesner, …, B. Honig. 2002. On the role of the crystal environment in determining protein side-chain conformations. *J. Mol. Biol.* 320:597–608.
41. Jacobson, M. P., G. A. Kaminski, …, C. S. Rapp. 2002. Force field validation using protein side chain prediction. *J. Phys. Chem. B.* 106:11673–11680.
42. Bahar, I., A. R. Atilgan, and B. Erman. 1997. Direct evaluation of thermal fluctuations in proteins using a single-parameter harmonic potential. *Fold. Des.* 2:173–181.
43. Kaminski, G. A., R. A. Friesner, …, W. L. Jorgensen. 2001. Evaluation and reparametrization of the OPLS-AA force field for proteins via comparison with accurate quantum chemical calculations on peptides†. *J. Phys. Chem. B.* 105:6474–6487.
44. Ghosh, A., C. S. Rapp, and R. A. Friesner. 1998. Generalized Born model based on a surface integral formulation. *J. Phys. Chem. B.* 102:10983–10990.
45. Tame, J. R. H., and B. Vallone. 2000. The structures of deoxy human haemoglobin and the mutant Hb Tyrα42His at 120 K. *Acta Crystallogr. D Biol. Crystallogr.* 56:805–811.
46. Silva, M. M., P. H. Rogers, and A. Arnone. 1992. A third quaternary structure of human hemoglobin A at 1.7-Å resolution. *J. Biol. Chem.* 267:17248–17256.
47. Cheng, X., and B. P. Schoenborn. 1990. Hydration in protein crystals. A neutron diffraction analysis of carbonmonoxymyoglobin. *Acta Crystallogr. B.* 46:195–208.
48. Schrödinger Suite. 2009. Protein Preparation Wizard; Epik version 2.0, S., LLC, New York, NY, 2009; Impact version 5.5, Schrödinger, LLC, New York, NY, 2009; Prime version 2.1, Schrödinger, LLC, New York, NY.
49. Kilmartin, J. V., J. J. Breen, …, C. Ho. 1973. Direct measurement of the pK values of an alkaline Bohr group in human hemoglobin. *Proc. Natl. Acad. Sci. USA.* 70:1246–1249.
50. Bettati, S., A. Mozzarelli, and M. F. Perutz. 1998. Allosteric mechanism of haemoglobin: rupture of salt-bridges raises the oxygen affinity of the T-structure. *J. Mol. Biol.* 281:581–585.
51. Schotte, F., J. Soman, …, P. A. Anfinrud. 2004. Picosecond time-resolved x-ray crystallography: probing protein function in real time. *J. Struct. Biol.* 147:235–246.
52. Head-Gordon, M., J. A. Pople, and M. J. Frisch. 1988. MP2 energy evaluation by direct methods. *Chem. Phys. Lett.* 153:503–506.
53. Sinnokrot, M. O., and C. D. Sherrill. 2004. Substituent effects in π-π interactions: sandwich and T-shaped configurations. *J. Am. Chem. Soc.* 126:7690–7697.
54. Schrödinger, LLC. 2011. QSite, version 5.7, Schrödinger, LLC, New York, NY.
55. Becke, A. D. 1986. Completely numerical calculations on diatomic molecules in the local-density approximation. *Phys. Rev. A.* 33:2786–2788.
56. Becke, A. D. 1988. Density-functional exchange-energy approximation with correct asymptotic behavior. *Phys. Rev. A.* 38:3098–3100.
57. Becke, A. D. 1993. A new mixing of Hartree-Fock and local density-functional theories. *J. Chem. Phys.* 98:1372–1377.
58. Becke, A. D. 1993. Density-functional thermochemistry. III. The role of exact exchange. *J. Chem. Phys.* 98:5648–5652.
59. Lee, C., W. Yang, and R. G. Parr. 1988. Development of the Colle-Salvetti correlation-energy formula into a functional of the electron density. *Phys. Rev. B Condens. Matter.* 37:785–789.
60. Hay, P. J., and W. R. Wadt. 1985. Ab initio effective core potentials for molecular calculations. Potentials for the transition metal atoms Sc to Hg. *J. Chem. Phys.* 82:270.
61. Hehre, W. J., R. Ditchfield, and J. A. Pople. 1972. Self consistent molecular orbital methods. XII. Further extensions of Gaussian-type basis sets for use in molecular orbital studies of organic molecules. *J. Chem. Phys.* 56:2257–2261.
62. Anselmi, M., A. Di Nola, and A. Amadei. 2008. The kinetics of ligand migration in crystallized myoglobin as revealed by molecular dynamics simulations. *Biophys. J.* 94:4277–4281.
63. Olson, J. S., J. Soman, and G. N. Phillips, Jr. 2007. Ligand pathways in myoglobin: a review of Trp cavity mutations. *IUBMB Life.* 59: 552–562.
64. Ruscio, J. Z., D. Kumar, …, A. V. Onufriev. 2008. Atomic level computational identification of ligand migration pathways between solvent and binding site in myoglobin. *Proc. Natl. Acad. Sci. USA.* 105:9204–9209.
65. Scott, E. E., and Q. H. Gibson. 1997. Ligand migration in sperm whale myoglobin. *Biochemistry.* 36:11909–11917.
66. Elber, R., and Q. H. Gibson. 2008. Toward quantitative simulations of carbon monoxide escape pathways in myoglobin. *J. Phys. Chem. B.* 112:6147–6154.
67. Lambright, D. G., S. Balasubramanian, and S. G. Boxer. 1989. Ligand and proton exchange dynamics in recombinant human myoglobin mutants. *J. Mol. Biol.* 207:289–299.
68. Chatfield, M. D., K. N. Walda, and D. Magde. 1990. Activation parameters for ligand escape from myoglobin proteins at room temperature. *J. Am. Chem. Soc.* 112:4680.
69. Tilton, Jr., R. F. J., U. C. Singh, …, D. A. Case. 1986. Computational studies of the interaction of myoglobin and xenon. *J. Mol. Biol.* 192:443–456.
70. Bossa, C., M. Anselmi, …, A. Di Nola. 2004. Extended molecular dynamics simulation of the carbon monoxide migration in sperm whale myoglobin. *Biophys. J.* 86:3855–3862.
71. Maragliano, L., G. Cottone, …, E. Vanden-Eijnden. 2009. Mapping the network of pathways of CO diffusion in myoglobin. *J. Am. Chem. Soc.* 132:1010–1017.
72. Guallar, V., A. A. Jarzecki, …, T. G. Spiro. 2006. Modeling of ligation-induced helix/loop displacements in myoglobin: toward an

understanding of hemoglobin allostery. *J. Am. Chem. Soc.* 128:5427–5435.

73. Samuni, U., D. Dantsker, …, J. M. Friedman. 2002. Spectroscopically and kinetically distinct conformational populations of sol-gel-encapsulated carbonmonoxy myoglobin. A comparison with hemoglobin. *J. Biol. Chem.* 277:25783–25790.
74. Adachi, S.-I., S.-Y. Park, …, N. Shibayama. 2003. Direct observation of photolysis-induced tertiary structural changes in hemoglobin. *Proc. Natl. Acad. Sci. USA*. 100:7039–7044.
75. Lepeshkevich, S. V., J. Karpiuk, …, B. M. Dzhagarov. 2004. A kinetic description of dioxygen motion within α- and β-subunits of human hemoglobin in the R-state: geminate and bimolecular stages of the oxygenation reaction. *Biochemistry.* 43:1675–1684.
76. Esquerra, R. M., R. A. Goldbeck, …, D. S. Kliger. 2000. Multiple geminate ligand recombinations in human hemoglobin. *Biophys. J.* 78: 3227–3239.
77. Sottini, S., S. Abbruzzetti, …, C. Viappiani. 2005. Geminate rebinding in R-state hemoglobin: kinetic and computational evidence for multiple hydrophobic pockets. *J. Am. Chem. Soc.* 127:17427–17432.
78. Schoenborn, B. P. 1965. Binding of xenon to horse haemoglobin. *Nature.* 208:760–762.